Origin of enhanced magnetoelectric coupling in $NiFe_2O_4/BaTiO_3$ multilayers studied by x-ray magnetic circular dichroism

V. K. Verma,[1,*,†] V. R. Singh,[1,‡] K. Ishigami,[1] G. Shibata,[1] T. Harano,[1] T. Kadono,[1] A. Fujimori,[1] F.-H. Chang,[2] H.-J. Lin,[2] D.-J. Huang,[2] C. T. Chen,[2] Yi Zhang,[3] Jing Liu,[3] Yuanhua Lin,[3] Ce-Wen Nan,[3] and A. Tanaka[4]

[1]*Department of Physics, University of Tokyo, Bunkyo-ku, Tokyo 113-0033, Japan*

[2]*National Synchrotron Radiation Research Center (NSRRC), Hsinchu 300, Taiwan*

[3]*State Key Lab of New Ceramics and Fine Processing, Department of Materials Science and Engineering, Tsinghua University, Beijing 100084, P. R. China*

[4]*Department of Quantum Matter, ADSM, Hiroshima University, Higashi-Hiroshima 739-8530, Japan*

(Received 15 January 2013; revised manuscript received 15 January 2014; published 25 March 2014)

$NiFe_2O_4/BaTiO_3$ (NFO/BTO) multilayer heterostructures grown on (001)-$SrTiO_3$ substrates with alternating ferroelectric BTO and ferrimagnetic NFO layers exhibit magnetoelectric (ME) coupling, which increases with the number of layers and, hence, with the number of NFO/BTO interfaces. We have studied the local electronic and magnetic states of Ni and Fe ions in the NFO/BTO multilayers with various NFO and BTO thicknesses by x-ray absorption spectroscopy and x-ray magnetic circular dichroism. With an increasing number of layers, both Ni and Fe magnetic moments decrease. With decreasing NFO layer thickness, the average magnetic moment of Ni decreases, while the average magnetic moment of Fe ions remains unaffected, meaning that Ni ions at the interface lose ferromagnetic moments. This suggests that the enhancement of ME coupling is associated with Ni ions at the interface whose ferromagnetic behavior is weakened through hybridization with the BTO electronic states.

DOI: 10.1103/PhysRevB.89.115128 PACS number(s): 75.70.−i, 73.21.Ac, 75.47.Lx, 75.85.+t

I. INTRODUCTION

Multiferroics, a class of materials that exhibit ferroelectric and ferromagnetic properties simultaneously, have drawn increasing interest due to their potential applications for next-generation multifunctional devices [1–4]. If there is magnetoelectric (ME) coupling in multiferroic materials, an external magnetic field will induce electric polarization, while an external electric field will induce magnetization. ME coupling in single-phase compounds is, however, generally weak. On the other hand, composite materials consisting of alternating ferroelectric and ferromagnetic layers [5] or ferromagnetic nano-rods embedded in a ferroelectric matrix [6,7] may exhibit stronger ME coupling.

Recently, thin films consisting of alternating ferromagnetic spinel-type $NiFe_2O_4$ (NFO) and ferroelectric perovskite-type $BaTiO_3$ (BTO) layers BTO/(NFO/BTO)$_n$ were prepared and exhibited the coexistence of ferroelectric and ferromagnetic ordering with strong ME coupling between them [8,9]. It was found that with increasing the number of layers n for a fixed total thickness of the sample, the magnetic moment decreases and ME coupling increases, and both observations were attributed to the NFO/BTO interfaces because the relative contributions of the interfaces increases with n. Structural compatibility of perovskites with various magnetic oxides, such as those with the spinel structures, allows one to combine thin layers of ferroelectric and magnetic materials to design multifunctional heterostructures. NFO is one of the well-known inverse spinel-structure oxides, represented by $Fe^{3+}[Ni^{2+}Fe^{3+}]O_4$. Half of the Fe^{3+} ions occupy the tetrahedral sites, while the Ni^{2+} ions and the other half of the Fe^{3+} ions occupy the octahedral sites. Similar to the antiferromagnetic coupling between Fe^{3+} ions at the tetrahedral and octahedral sites in Fe_3O_4, the Ni^{2+} ions at the octahedral sites and the Fe^{3+} ions at the tetrahedral sites are antiferromagnetically coupled through superexchange interaction via oxygen ions, as the Kanamori-Goodenough rule predicts [10,11].

To understand the microscopic origin of the enhanced ME coupling at the BTO/NFO interfaces in the BTO/NFO multilayer thin films, it is necessary to investigate the electronic and magnetic properties of the Fe and Ni ions at the interfaces. For that purpose, x-ray absorption spectroscopy (XAS) and x-ray magnetic circular dichroism (XMCD) are ideal techniques because they are element-specific probes of the electronic and magnetic properties of transition-metal ions [12]. We have studied the Fe and Ni ions in samples with various BTO and NFO layer thicknesses. We have found that interfacial Ni atoms lose ferromagnetic moment while the Fe magnetic moments remain unaffected at the interface, and the loss of the Ni ferromagnetic moment is correlated with the enhancement of ME coupling in the NFO/BTO multilayers. We discuss how both the weakened Ni ferromagnetic moment and the enhanced ME coupling can simultaneously be realized at the interface.

II. EXPERIMENTAL

Two sets of BTO/(NFO/BTO)$_n$ ($n = 1, 2, 3, 4$) multilayers were prepared on (001)-oriented 0.7% Nb-doped $SrTiO_3$ (STO) single-crystal substrates by using the pulsed laser deposition technique. BTO and NFO ceramic targets were used to prepare the BTO and NFO multilayers. The KrF laser with a power density of 1.5 J/cm^2 and a flowing oxygen pressure of 13 Pa were maintained. During the deposition, the pulse repetition rate of 2–4 Hz and the substrate temperature of

*Corresponding author: vkverma@wyvern.phys.s.u-tokyo.ac.jp

†Present address: Department of Physics, Madanapalle Institute of Technology & Science, Angallu, Madanapalle-517325, AP, India.

‡Present address: Department of Physics and Astronomy, University of Nebraska-Lincoln, NE 68588-0299, USA.

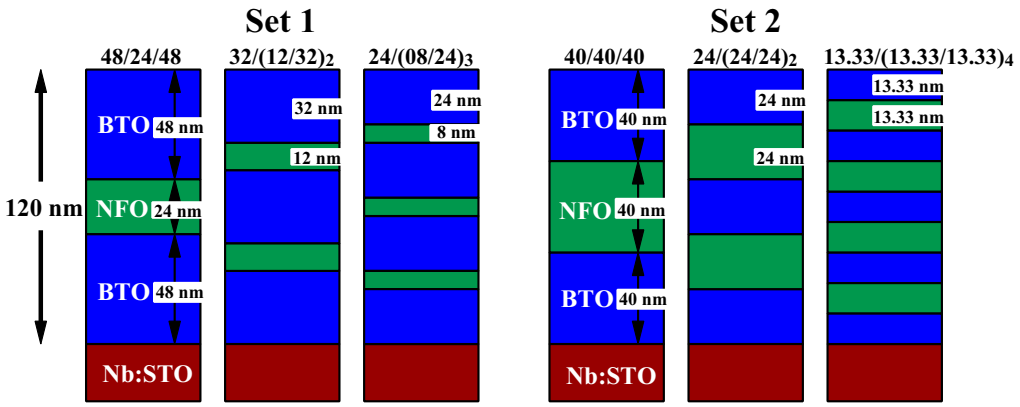

FIG. 1. (Color online) Sample structures of BTO/(NFO/BTO)$_n$ multilayer thin films. In set 1 samples, the volume ratios of BTO to NFO are kept to 4:1, while in set 2 samples, the thicknesses of the BTO and NFO layers are the same in each sample.

800 °C were used. The deposited films were then annealed at 800 °C for 1 hour at 3000 Pa oxygen pressure. The prepared high quality samples were characterized for their properties using x-ray diffraction and scanning electron microscopy [9]. The structures of the samples are shown in Fig. 1. The total thicknesses of these films were kept at about 120 nm. We prepared two sets of samples. In set 1, the volume ratios of BTO to NFO in the films are kept at 4:1, while in set 2, the thicknesses of the NFO and BTO layers were the same. The thickness ratio of BTO to NFO, therefore, varies between samples.

The XAS and XMCD measurements were carried out at the Dragon beamline 11A of National Synchrotron Radiation Research Center (NSRRC), Taiwan. XAS and XMCD spectra were collected in the total-fluorescence-yield mode by using a photodiode. Because the probing depth of the fluorescence detection is about 100 nm, the entire volume of the multilayers was probed. In order to obtain XMCD spectra, the direction of the applied magnetic field was reversed. That is, XAS spectra for positive and negative magnetic field directions $\mu_\pm$ with fixed photon helicity were taken, and XAS and XMCD spectra were obtained by taking the average and the difference between μ_+ and μ_-, respectively. To obtain XMCD in a magnetic field less than 1 T accurately and reproducibly, we always set the magnetic field +1 T and −1 T before we set lower magnetic field. (For example, in order to obtain μ_+ and μ_- XAS at 0.5 T, we set +1 T then +0.5 T, and we set −1 T then −0.5 T. Similarly, to obtain the remanent magnetization at zero field, we set +1 T then 0 T, and we set −1 T then 0 T, respectively.) The L_3 edge of XAS has been normalized to unity by dividing the average of μ_+ and μ_- XAS and XMCD scaled consistently. The magnetic field was parallel to the surface plane of the samples and made an angle of 30° with respect to the Poynting vector of the soft x rays. All the measurements were performed at room temperature with magnetic fields up to 1 T. The base pressure of the chamber was about 1×10^{-9} Torr.

III. RESULTS AND DISCUSSION

Figure 2 shows the Fe $L_{2,3}$ XAS and XMCD spectra of the BTO/NFO/BTO film ($n = 1$) of set 1. The spin-orbit coupling of the Fe $2p$ core level splits the XAS into the L_3 ($2p_{3/2}$) and L_2 ($2p_{1/2}$) edges separated by ∼13 eV. In Fig. 2(a), the Fe $L_{2,3}$ XAS spectrum of the BTO/NFO/BTO film is compared with those of Fe metal [18], $GaFeO_3$ [19], and γ-Fe_2O_3 [20]. The valance state of Fe in γ-Fe_2O_3 and $GaFeO_3$ are all trivalent, but the Fe ions are located at sites of different local symmetries. The line shape of the Fe $L_{2,3}$ XAS spectrum of BTO/NFO/BTO is rather similar to both γ-Fe_2O_3 and $GaFeO_3$ but is quite different from that of Fe metal, indicating that the valence of the Fe ions in BTO/NFO/BTO are in 3+. The difference of the XAS of BTO/NFO/BTO from those of γ-Fe_2O_3 and $GaFeO_3$ is the lower intensities of structures A and C in BTO/NFO/BTO. Because peaks A and C are due to Fe^{3+} ions at the octahedral (O_h) sites and peak B to those at the tetrahedral (T_d) site, weaker A and C mean that the number of Fe^{3+} at the octahedral positions is smaller. This corresponds to the facts that the octahedral-to-tetrahedral ratio decreases from 5:3 in γ-Fe_2O_3 to 1:1 in NFO, and all the Fe^{3+} ions occupy the (distorted) octahedral sites in $GaFeO_3$. Note that γ-Fe_2O_3 has the spinel structure represented by $Fe^{3+}[\square_{1/3}Fe^{3+}{}_{5/3}]O_4$, where the open square denotes Fe (O_h) vacancies, and that NFO is represented by $Fe^{3+}[Ni^{2+}Fe^{3+}]O_4$.

The different sites of Fe^{3+} become much more evident in XMCD. The Fe L_3 XMCD spectra of the BTO/NFO/BTO samples show three sharp negative, positive, and negative peaks at $h\nu = 708.15$, 709.30, and 710.25 eV, respectively, denoted by A, B, and C. The positive and negative peaks correspond to the directions of the spins of the Fe^{3+} ions at the tetrahedral and octahedral sites, which are coupled antiferromagnetically in NFO. The negative peaks A and C come from the Fe^{3+} ions at the octahedral sites, and the positive peak B comes from the Fe^{3+} ions at the tetrahedral sites. The XMCD spectrum is also compared with those of γ-Fe_2O_3, $GaFeO_3$ and Fe metal. The XMCD spectral line shape of the BTO/NFO/BTO sample is clearly different from that of Fe metal. The positive peak B due to Fe^{3+} at the T_d sites is absent in $GaFeO_3$ because all the Fe^{3+} ions occupy the octahedral sites in $GaFeO_3$. The peak positions of A, B, and C coincide with those of γ-Fe_2O_3, indicating that Fe^{3+} ions are both at the T_d and O_h sites. Peak C is weaker in NFO because of the smaller $Fe^{3+}(O_h)$ to $Fe^{3+}(T_d)$ ratio than γ-Fe_2O_3.

In Fig. 3, the XAS and XMCD spectra of the Ni $L_{2,3}$ core level are shown and are compared with the spectra of reference compounds. Each absorption spectrum of Ni shows two groups, the L_3 ($2p_{3/2}$) and L_2 ($2p_{1/2}$) edges, separated by the spin-orbit splitting of the $2p$ core level of ∼17 eV.

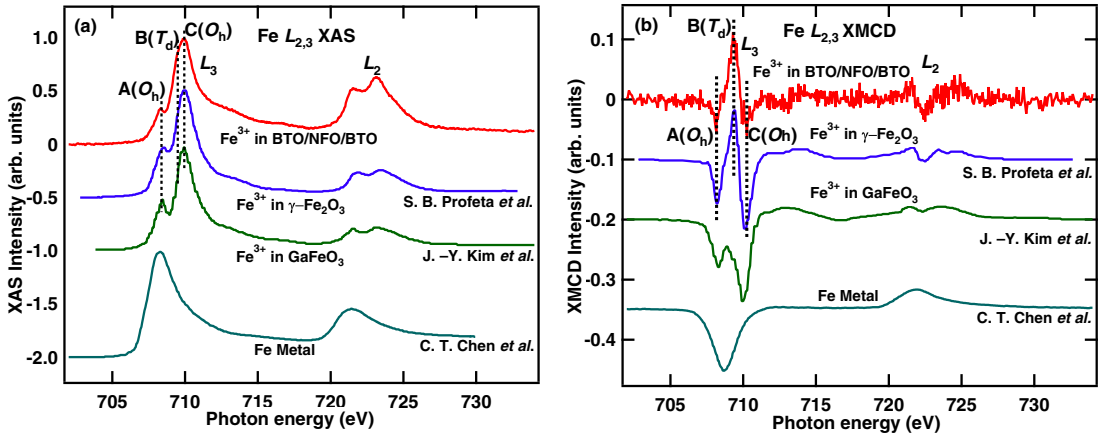

FIG. 2. (Color online) Comparison of the Fe $L_{2,3}$ XAS (a) and XMCD (b) spectra of the BTO/NFO/BTO thin film of set 1 with those of Fe metal [18], $GaFeO_3$ [19], and γ-Fe_2O_3 [20].

The double peak structure at the L_3 edge and a partially resolved doublet structure at the L_2 edge are the characteristic features of the high spin ($S = 1$) Ni^{2+} ion in the octahedral crystal field [13,14]. In panel (a), the Ni $L_{2,3}$ XAS spectrum measured for the BTO/NFO/BTO sample is compared with the reference data of Ni metal [15], $PrNiO_3$ (Ni^{3+}) [16], NiO (Ni^{2+}) [17], and a calculated spectrum of Ni^{2+} in an octahedral crystal field. The Ni $L_{2,3}$ XAS spectrum of BTO/NFO/BTO is different from those of Ni metal and $PrNiO_3$ and similar to the spectrum of NiO and the calculated spectrum of Ni^{2+} in an octahedral crystal field, indicating that the valance of Ni in BTO/NFO/BTO is 2+ like Ni in NiO. As for XMCD, as shown in Fig. 3(b), the Ni $L_{2,3}$ XMCD spectrum of BTO/NFO/BTO is different from that of Ni metal and agrees well with the calculated XMCD spectrum of Ni^{2+} in the octahedral crystal field (10 Dq = 1.5 eV), indicating that the ionic Ni atoms with localized 3*d* electrons contribute to the magnetism in the present sample.

Figures 4(a) and 4(b) show the Fe and Ni $L_{2,3}$ XMCD spectra of the BTO/NFO/BTO thin film of set 1 measured at magnetic fields 0.2, 0.5, and 1 T. Figure 4(c) shows the Fe L_3 XMCD intensities at peaks A and B, which are assigned to Fe^{3+} ions at the O_h and T_d sites, respectively, and Fig. 4(d) shows comparison of the Ni L_3 XMCD intensity with the magnetization measured using a superconducting quantum interference device (SQUID) magnetometer. The magnetic field dependence of the XMCD spectra of the BTO/NFO/BTO thin film indicates residual magnetization at zero field and clearly shows ferromagnetism at room temperature. The remanent magnetization at zero field was about 23% of the saturation magnetization. The magnetic hysteresis loop of BTO/(NFO/BTO)$_n$ samples have been published by Liu *et al.* [9]. As a result, the saturation magnetization, remnant magnetization, and coercivity decrease with the increase of the number of interfaces.

Figure 5 shows how the XMCD spectra change between the different samples having different numbers and thicknesses of NFO and BTO layers. The XMCD spectra of set 1 at the Fe and Ni $L_{2,3}$ edges of various *n*s are shown in Figs. 5(a) and 5(b). The XMCD intensity of the Fe and Ni $L_{2,3}$ edges decreases with increasing number of NFO and BTO layers, as shown in Figs. 5(c) and 5(d). This observation means that as we increase the interface volume ratio of the NFO layers, the magnetization decreases, which implies the degradation of the

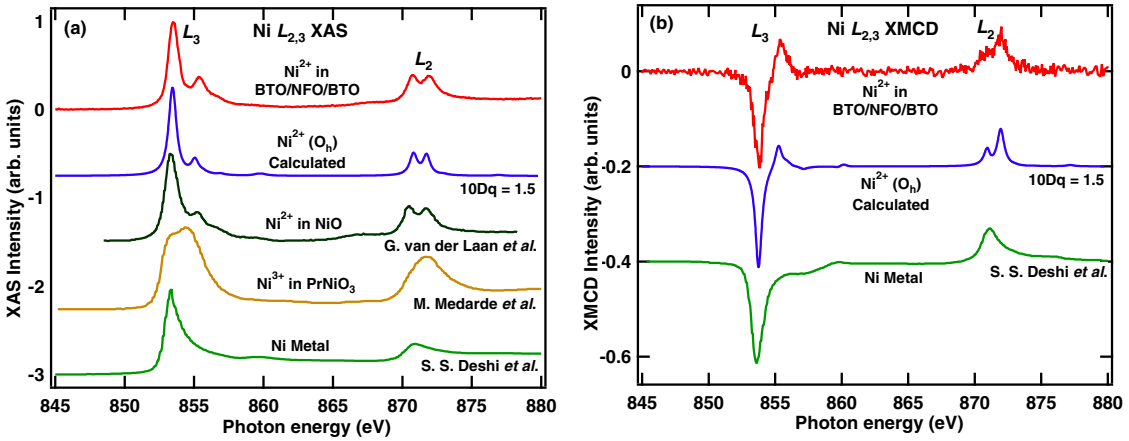

FIG. 3. (Color online) Comparison of the Ni $L_{2,3}$ XAS (a) and XMCD (b) spectra of the BTO/NFO/BTO thin film of set 1 with those of Ni metal [15], $PrNiO_3$ (Ni^{3+}) [16], NiO (Ni^{2+}) [17], and the calculated spectra of Ni^{2+} in an octahedral crystal field.

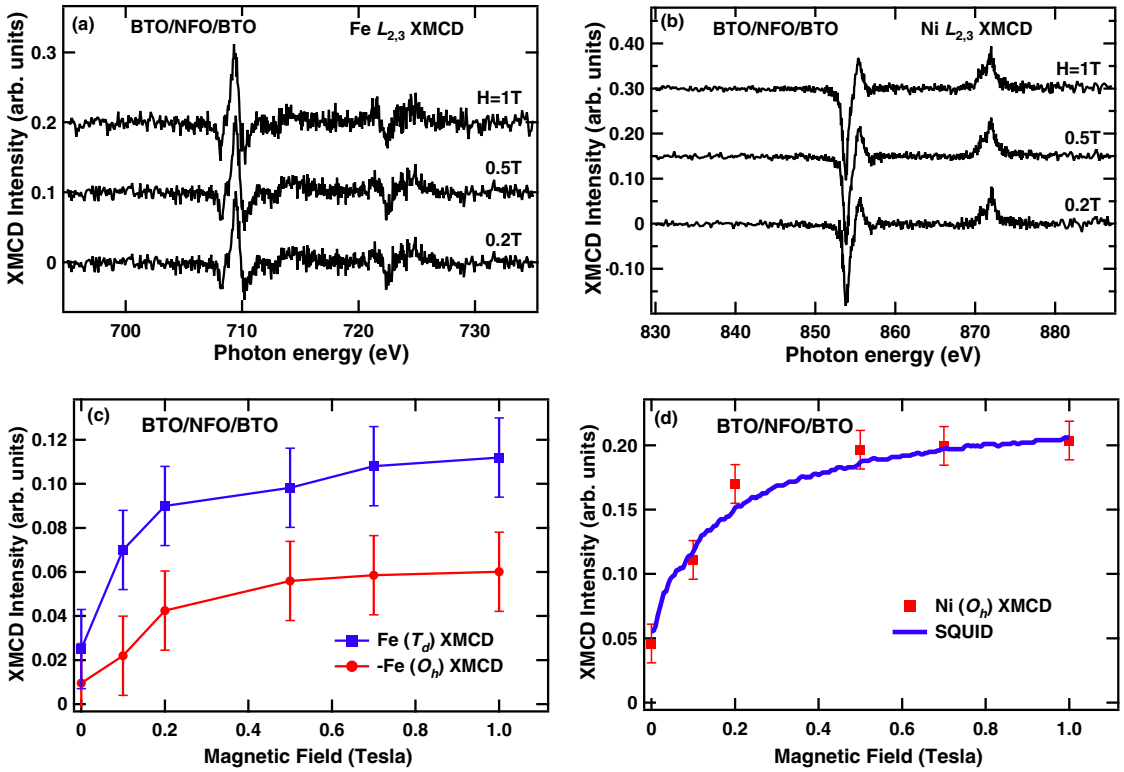

FIG. 4. (Color online) Fe (a) and Ni (b) $L_{2,3}$ XMCD spectra of the BTO/NFO/BTO thin film of set 1 at various magnetic fields. (c) Fe L_3 XMCD intensities at peaks A and B, which are assigned to Fe^{3+} ions at the O_h and T_d sites, respectively. (d) Comparison of the SQUID results with the Ni L_3 XMCD intensity of BTO/NFO/BTO.

Ni ferromagnetic moment at the interfaces. Figure 5(e) shows the ME coupling coefficient α_E versus the number of layers of the BTO/(NFO/BTO)$_n$ thin films of sets 1 and 2. Here, α_E is defined by $\delta V/(\delta H t)$, where δV is the induced voltage signal, δH is the magnetic excitation signal, and t is the total film thickness. With the increase of number of layers, the ME coupling coefficient α_E increases. From Figs. 5(c), 5(d), and 5(e), we can conclude that when the magnetic moment of Ni and Fe decreases, the ME coupling increases. By changing the layer numbers, not only the interfaces but also the strain from the BTO layer may influence the magnetization of NFO because the NFO layers would be in a highly compressively strained state due to the lattice mismatch between the NFO and BTO layers. Liu *et al.* [9] showed that when the number of layers increases, the c parameter of NFO increases, as shown in Fig. 6(c), which means that the compressive strain within the a-b plane in NFO layers increases. We also obtained a similar trend of decreasing magnetization for set 2 of BTO/(NFO/BTO)$_n$ multilayer thin films, but set 1 and set 2 behave differently as functions of the layer (interface) number, which indeed indicates that the strain also affects the magnetization in a complicated way.

In order to see how the Ni and Fe magnetizations are affected by the interface and the strain, we have plotted the percentage of the L_3 edge XMCD intensities of Fe and Ni against the NFO layer thickness (x axis) and the layer number $2n + 1$ (y axis) in Figs. 6(a) and 6(b) on the color scale. Here, appropriate interpolation and extrapolation have been made for the color coding. In the x (NFO thickness) direction, as the NFO layer thickness increases, the interfacial volume ratio of the NFO layer decreases. In the y (layer number) direction, the compressive strain (or lattice distortion) in the NFO layer increases according to the data from Liu *et al.* [9] as replotted in Fig. 6(c). The gradual reduction of the magnetization in the BTO/NFO/BTO multilayers with layer number could be understood by considering the negative magnetostriction of NFO that it contracts when magnetized [21]. Figures 6(a) and 6(b) show that the Fe L_3 XMCD intensity depends only on the layer number, while the Ni L_3 XMCD intensity depends on both the layer number and NFO thickness. This means that both Fe and Ni ferromagnetic moments decrease due to strain, while the Ni ferromagnetic moment decreases additionally at the interface. The fact that the decrease of the Ni dichroism signal with decreasing thickness of the NFO layer occurs on top of the decrease of both Fe and Ni dichroism signals with the total number of the layers indicates that the decrease of the Ni moment occurs at the interface and not over many layers. To check this, we have estimated the dead layer thickness to be as thin as 2–4 nm from the decrease of the Ni XMCD to Fe XMCD intensity ratio, confirming our original assumption.

As for the ME coupling, multilayers consisting of NFO and BTO layers clearly yields ME output, which increases with the layer number [9]. The interface therefore should play a crucial role in inducing the ME coupling. In Fig. 6(d), the ME voltage coefficient α_E is plotted as a function of the NFO thickness and the layer number. From comparison of Figs. 6(b) and 6(c), it is clear that ME coupling increases with the decrease of Ni ferromagnetism at the interface. A

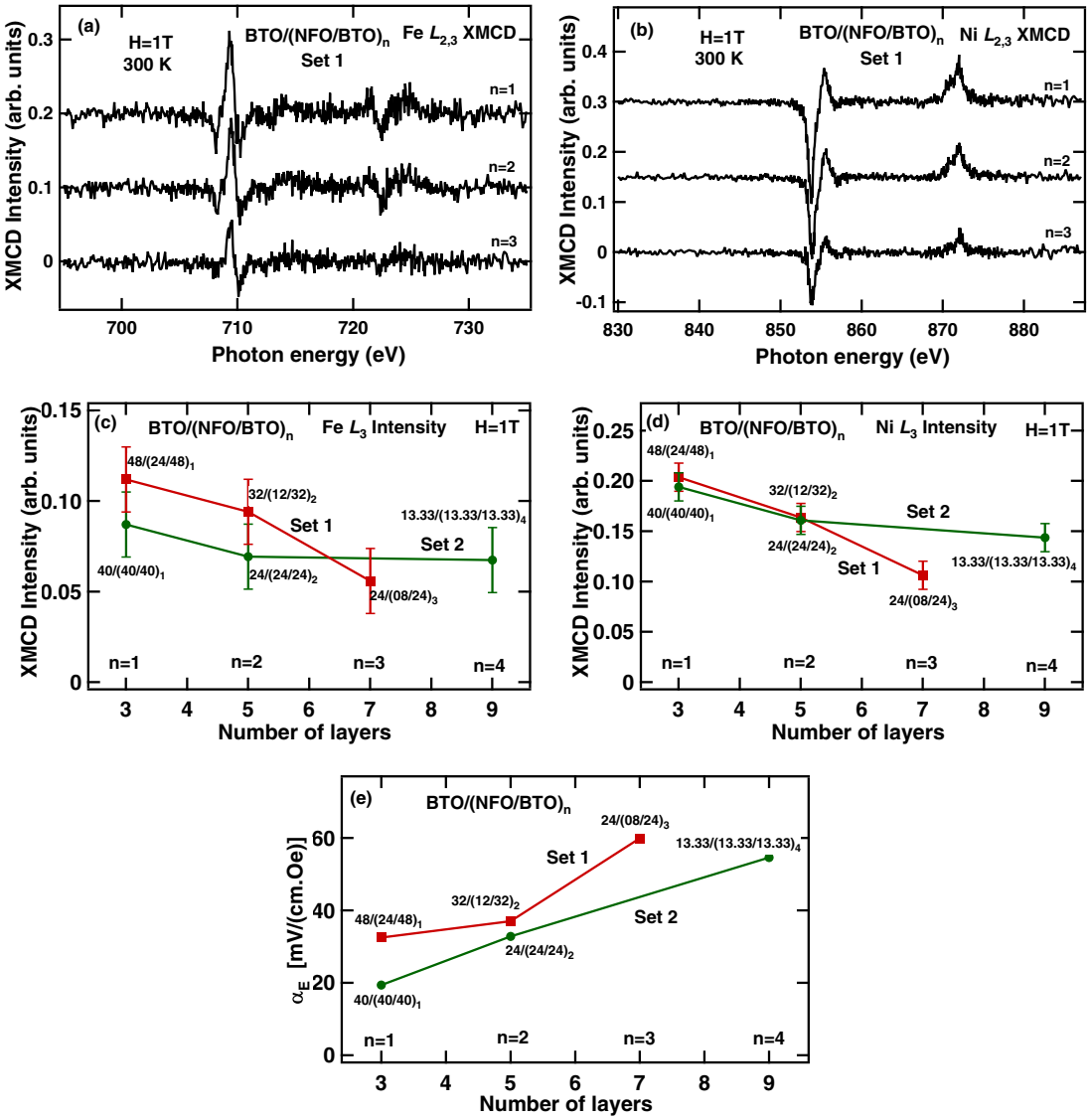

FIG. 5. (Color online) Fe (a) and Ni (b) $L_{2,3}$ XMCD spectra of the BTO/(NFO/BTO)$_n$ thin films (where $n = 1, 2, 3$) of set 1. The Fe L_3 XMCD intensities (c), Ni L_3 XMCD intensities (d), and ME coupling coefficient α_E (e) versus the number of layers of the BTO/(NFO/BTO)$_n$ thin films of sets 1 and 2.

possible cause of the reduction of the Ni spin moment at the interface is spin canting. Chinnasamy *et al.* [22] deducted a noncollinear magnetic structure on the surface of ultrafine particles using Mossbauer spectroscopy, magnetization, and EXAFS measurements and observed the canting of surface spins. Aguesse *et al.* [23] discussed atomic diffusion across the interface between $CoFe_2O_4$ (CFO) and BTO layers. In the present case, atomic diffusion between NFO and BTO appears more likely because of the analogy to the CFO/BTO system.

Recently, microscopic mechanism of ME coupling at the Fe/BTO interface was studied by element specific x-ray magnetic scattering, and Ti atoms at the interface were found to have finite spin polarization [24]. The details about the nature of the ME coupling in the NFO/BTO multilayers are currently unknown, but we speculate that strong ME coupling occurs at the interface defects, where Ni atoms of NFO and Ti atoms of BTO are located close and hybridizing each other (probably through intervening oxygen atoms) and the magnetic moments of the Ni atoms is partially transferred to Ti atoms. It is also a possible scenario that some Ni atoms are diffused out of the NFO layer into the BTO layer and replace Ti atoms. In the latter case, contributions of Ni to the ferromagnetism will be weakened, while the Fe atoms will remain ferromagnetically order through the robust superexchange coupling between the $Fe^{3+}(O_h)$ and $Fe^{3+}(T_d)$. The magnetic moments of the Ni atoms and the ferroelectric distortion of the BTO lattice will thus have finite coupling and enhance the ME coupling in the NFO/BTO interfacial regions.

IV. CONCLUSIONS

Multilayer heterostructures BTO/(NFO/BTO)$_n$ epitaxially grown on (001)-STO substrates were studied by XAS and XMCD. The Ni ions are in the 2+ states at the O_h position, while Fe ions are in the 3+ states at O_h and T_d positions of the spinel structure. The ferromagnetic moment of Ni^{2+} is

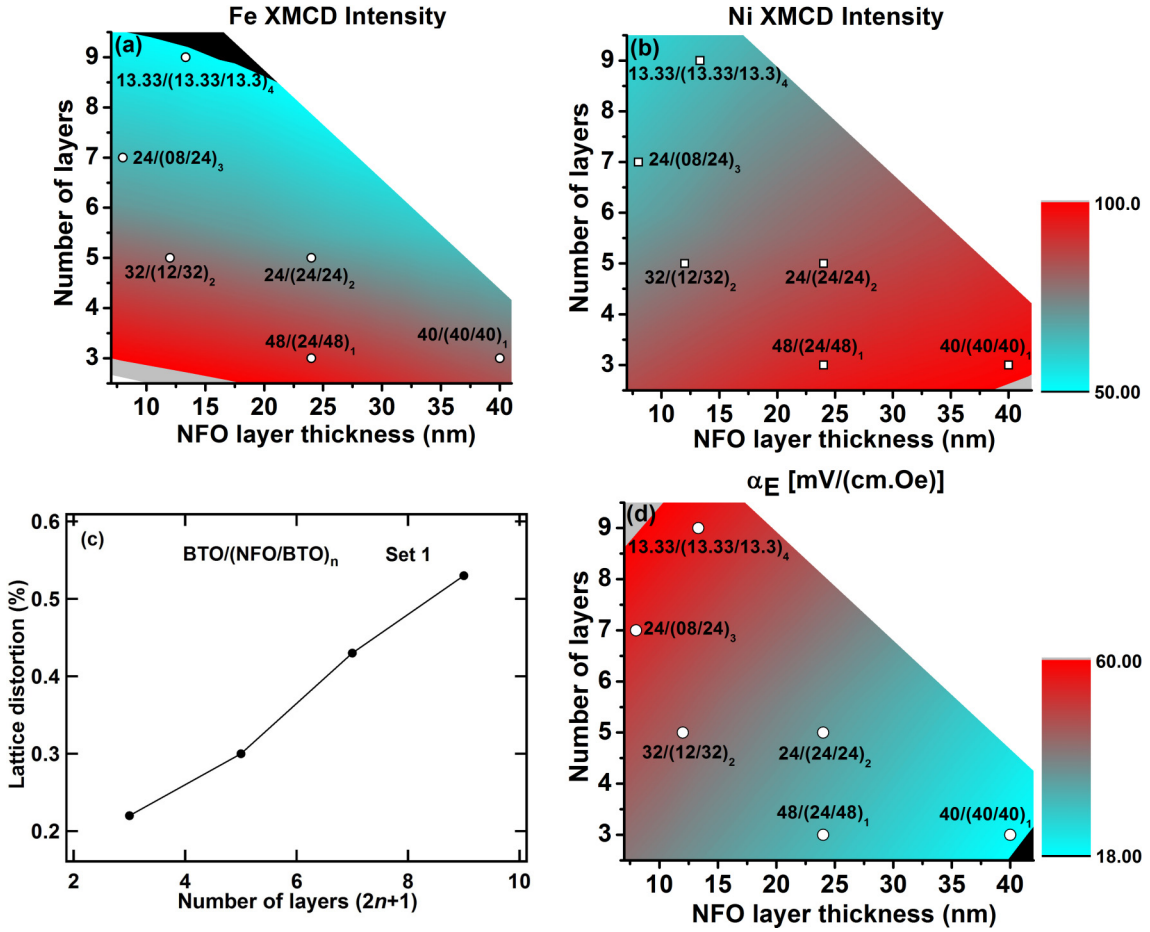

FIG. 6. (Color online) Fe (a) Ni (b) L_3 XMCD intensity plotted against the NFO thickness and the layer number $2n + 1$. (c) Lattice distortion $(c_{\mathrm{NFOlayer}} - c_{\mathrm{NFObulk}})/c_{\mathrm{NFObulk}}$ versus the number of layers of set 1 samples [9]. (d) ME coupling coefficient α_E plotted against the NFO thickness and the layer number.

parallel to $Fe^{3+}(O_h)$ but are antiparallel to $Fe^{3+}(T_d)$ following the inverse spinel structure of NFO. The Ni ferromagnetic moment is found to decrease at the interface. We found clear correlation between the ME coupling strength and the decreases of the ferromagnetic moment of Ni. This suggests that the enhancement of ME coupling occurs through interfacial Ni atoms or Ni atoms diffused into the BTO side, whose hybridization with the BTO electronic states is enhanced and whose ferromagnetic behavior is weakened.

ACKNOWLEDGMENTS

This work was supported by a Grant-in-Aid for Scientific Research (S22224005) from JSPS, for Scientific Research in Priority Area "Creation and Control of Spin Current" (19048012) from MEXT, and a Global COE Program from MEXT, Japan. The work in China was supported by the NSF of China (Grants No. 50921061 and No. 51025205) and the National Basic Research Program of China (973-Program, Grant No. 2009CB623303).

[1] W. Eerenstein, N. D. Mathur, and J. F. Scott, Nature **442**, 759 (2006).

[2] X. L. Zhong, J. B. Wang, M. Liao, G. J. Huang, S. H. Xie, Y. C. Zhou, Y. Qiao, and J. P. He, Appl. Phys. Lett. **90**, 152903 (2007).

[3] R. Y. Zheng, J. Wang, and S. Ramakrishna, J. Appl. Phys. **104**, 034106 (2008).

[4] V. R. Singh, A. Garg, and D. C. Agrawal, Appl. Phys. Lett. **92**, 152905 (2008).

[5] J. Ma, J. Hu, Z. Li, and C-W. Nan, Adv. Mater. **23**, 1062 (2011).

[6] H. Zheng, J. Wang, S. E. Lofland, Z. Ma, L. Mohaddes-Ardabili, T. Zhao, L. Salamanca-Riba, S. R. Shinde, S. B. Ogale, F. Bai, D. Viehland, Y. Jia, D. G. Schlom, M. Wuttig, A. Roytburd, and R. Ramesh, Science **303**, 661 (2004).

[7] R. Ramesh and Nicola A. Spaldin, Nat. Mater. **6**, 21 (2007).

[8] C. Deng, Y. Zhang, J. Ma, Y. Lin, and C. W. Nan, J. Appl. Phys. **102**, 074114 (2007).

[9] J. Liu, Y. Zhang, Y. Lin, and C. W. Nan, J. Appl. Phys. **105**, 083915 (2009).
[10] J. Kanamori, J. Phys. Chem. Solids **10**, 87 (1959).
[11] J. B. Goodenough, Phys. Rev. **100**, 564 (1955).
[12] V. R. Singh, Y. Sakamoto, T. Kataoka, M. Kobayashi, Y. Yamazaki, A. Fujimori,F.-H. Chang, D.-J. Huang, H.-J. Lin, C. T. Chen, H. Toyosaki, T. Fukumura, and M. Kawasaki, J. Phys.: Condens. Matter **23**, 176001 (2011),
[13] H. Wang, D. S. Patil, C. Y. Ralston, C. Bryant, and S. P. Cramer, J. Electron Spectrosc. Relat. Phenom. **114**, 865 (2001).
[14] G. van der Laan, B. T. Thole, G. A. Sawatzky, and M. Verdaguer, Phys. Rev. B **37**, 6587 (1988).
[15] S. S. Dhesi, E. Dudzik, H. A. Durr, N. B. Brookes, and G. van der Laan, Surf. Sci. **454**, 930 (2000).
[16] M. Medarde, A. Fontaine, J. L. García-Muñoz, J. Rodríguez-Carvajal, M. De Santis, M. Sacchi, G. Rossi, and P. Lacorre, Phys. Rev. B **46**, 14975 (1992).
[17] G. van der Laan, J. Zaanen, G. A. Sawatzky, R. Karnatak, and J.-M. Esteva, Phys. Rev. B **33**, 4253 (1986).
[18] C. T. Chen, Y. U. Idzerda, H.-J. Lin, N. V. Smith, G. Meigs, E. Chaban, G. H. Ho, E. Pellegrin, and F. Sette, Phys. Rev. Lett. **75**, 152 (1995).
[19] J.-Y. Kim, T. Y. Koo, and J.-H. Park, Phys. Rev. Lett. **96**, 047205 (2006).
[20] S. B. Profeta, M.-A. Arrio, E. Tronc, N. Menguy, I. Letard, C. C. D. Moulin, M. Nogues, C. Chaneac, J.-P. Jolivet, and P. Sainctavit, J. Magn. Magn. Mater. **288**, 354 (2005).
[21] D. Fritsch and C. Ederer, Phys. Rev. B **86**, 014406 (2012).
[22] C. N. Chinnasamy, A. Narayanasamy, N. Ponpandian, K. Chattopadhyay, K. Shinoda, B. Jeyadevan, K. Tohji, K. Nakatsuka, T. Furubayashi, and I. Nakatani, Phys. Rev. B **63**, 184108 (2001).
[23] F. Aguesse, A.-K. Axelsson, M. Valantb, and N. M. Alford, Scr. Mater. **67**, 249 (2012).
[24] S. Valencia, A. Crassous, L. Bocher, V. Garcia, X. Moya, R. O. Cherifi, C. Deranlot, K. Bouzehouane, S. Fusil, A. Zobelli, A. Gloter, N. D. Mathur, A. Gaupp, R. Abrudan, F. Radu, A. Barthelemy, and M. Bibes, Nat. Mater. **10**, 753 (2011).